Numerical Analysis of Time-Dependent Strength and Stiffness in Palm Oil Fuel Ash-Stabilized Soil: Early and Long-Term Effects

Nour A. W. Al-Dalain [1], Ali M. A. Ezreig [1], Mohd A. M. Ismail [1*]

[1] School of Civil Engineering, Engineering Campus, Universiti Sains Malaysia, 14300, Pulau Pinang, Malaysia.

Abstract

Over the years, investigating the behavior of soft soil, stabilized using different techniques, has been recognized as a critical priority for geotechnical engineers. Numerous soil constitutive models have been utilized to simulate stabilized soil behavior, improve strength and ductility, and analyze load-deformation responses. However, further investigation is required to study stabilized soil's time-dependent strength and stiffness, especially at an early curing age. Early strength and stiffness development is crucial in engineering construction for improving building quality and efficiency and minimizing crack risk. Furthermore, estimating UCS from an early age aid in safety evaluation and ground-improvement analysis. Researchers are increasingly recognizing palm oil fuel ash (POFA) as an eco-friendly alternative to traditional soil stabilizers due to its abundant availability. This study proposes an advanced concrete constitutive model to simulate the time-dependent strength and stiffness of POFA-stabilized and cement-stabilized soil due to pozzolanic interactions. The model accurately measures strength and stiffness improvement from an early curing age to 28 days using finite element analysis (FEA) before then comparing the experimental results. Based on the experimental results, the UCS values of palm oil fuel ash-stabilized soil grew to 3.18 MPa and 3.89 MPa after seven and 28 days with an optimum content of 30% (POFA): 10% Magnesium Oxide (MgO). It exhibited a significant increase in early strength with 64.02% compared with cement-stabilized soil. For stiffness results, a slight increment of 9.26% was observed. Employing FEM, the sensitivity of the parameters to stress-strain behavior was investigated. Finally, the validity of the concrete constitutive model to predict the time-dependent strength and stiffness of stabilized soil was proved.

Keywords: Soil Stabilisation; Time-Dependent Strength and Stiffness; Unconfined Compressive Strength (UCS); Elastic Modulus (E).

1. Introduction

Research on soil has a long tradition. Soil is a complex material that exhibits non-linear behavior and often produces time-dependent behavior when subjected to stress. The complexity of soil behavior stems from its composition as a multi-phase material, showcasing a range of characteristics. These include elastic, plastic, and non-linear deformations, as well as the presence of plastic and failure deformations [1]. Several soil models have been established, and these can be categorized into elasto-plastic, elastovisco-plastic, linear, and non-linear elastic [2, 3]. The development of soil constitutive models has become an imperative priority in providing a more precise and accurate comprehension of soil mechanics and the way in which soil interacts with different loads and environmental circumstances. The use of such models also provides a faster process, which costs less than experimental testing.

Different constitutive models have been developed to simulate soil behavior over time, such as rate dependency, stress relaxation, and creep behavior [4]. The elastic-viscoplastic model was used to capture the time-dependent behavior of soft, saturated clay. Scholars such as Karstunen & Yin [5] and Baskari et al. [6] used the soil rheology constitutive models to evaluate the creep behavior of Cillian volcanic clay and to estimate the reduction in soil-strength parameters over time. Despite that, the broader adoption of elastovisco-plastic (EVP) analysis among geotechnical engineers remains limited. This is mainly due to the complex mathematical formulation of constitutive models, require of soil parameters, and difficulties in identifying them [4]. Mohr-Coulomb, Soft Soil, Hardening Soil, and Soft Soil Creep models have been utilized to model soil behavior [7]. The elastoplastic model was used by Sternik [8] to simulate the reduction of stiffness for over-consolidated clay under triaxial loading. To align with the requirements for various development goals, soil-quality improvement has been widely investigated. In the last few years, the behavior of stabilized soil has been predicted numerically using different constitutive models [9–11]. The vertical deformation of cement-stabilized soft soil was analyzed using FEM by Tsige et al. [12].

Moreover, the effect of utilizing waste materials as soft-soil stabilizers on vertical displacement was investigated [13–15]. The study, conducted by Adithan et al. [16], determined the optimum content of Quarry Dust Powder to produce less settlement of reinforced soil using the Mohr-Coulomb model. Robin et al. [17] used the Modified Cam Clay model to observe the modification of mechanical parameters due to lime treatment. Nguyen et al. [18] also used the Modified Cam Clay model to predict the failure behavior of fiber-reinforced cement-treated clay. 3D finite element analysis was achieved to simulate the rutting behavior of the soil stabilized with foamed sulphur asphalt [19].

Due to drying shrinkage, shrinkage cracking of cement-stabilized materials is likely to occur, leading Li [20] to predict cemented soil's shrinkage cracking and shrinkage stress. The prediction of the time-dependent strength and stiffness of the stabilized soil due to pozzolanic reactions requires an accurate constitutive model. The improvement of Young's modulus up to the age of 28 days in the soil stabilized with fly ash was simulated using the Mohr column model by Mahvash-Mohammadi [21]. Although the behavior of stabilized soil has been described previously using different constitutive models, very limited investigations on the time-dependent strength and stiffness of stabilized soil have been reported to date, especially at the early age of curing. In this study, the concrete constitutive model was used, developed by Shaalan et al. [22].

A concrete model was proposed based on elastic-plastic structure to capture the strain behavior of materials based on cement, including elastic, plastic, creep, and shrinkage strains [23]. It was initially created for use in tunnelling applications where the time-dependent behavior of shotcrete is estimated by estimating stress-strain behavior [24, 25]. It has the capability to investigate the strength of shotcrete at an early age. The characteristics of this model were examined as a relevant approach to simulating cement-treated soil behavior by applying it to DSM columns in waterway construction in Singapore with negligence of time-dependency behavior. It was revealed that it had the ability to model strain-softening characteristics [26]. The concrete model was used in another study, conducted by Hung et al. [27], to simulate the hardening and softening behaviors of cement soil columns in Singapore. According to the results, a good degree of agreement has been achieved between the modeling of the concrete model and the test findings.

The capability of concrete models to design and model geotechnical reinforced concrete structures more precisely was investigated by Maatkamp [28]. One of the most important aspects of engineering construction is the development of early compressive strength. This significantly improves building quality and efficiency in construction, minimizes the risk of early cracks, and allows for earlier use of the building [29–32]. In this proposed model, the early strength and stiffness of stabilized soil, in particular, were simulated. Over the years, soil stabilization was achieved using ordinary Portland cement as a conventional method. High production costs, high energy use, and CO_2 emissions, contributing to global warming, are all justifications for researchers to look for the most cost-effective and eco-friendly cement substitutes in soil stabilization [33, 34]. Recently, utilization of waste materials for soil stabilization has been increasingly achieved by geotechnical engineers [35–37].

POFA has been extensively used and studied among the many waste materials that enhance soil properties. It is a byproduct of burning palm kernel shells and palm oil husks in biomass power plants and is one of the most common types of waste produced in Malaysia. In 2009–2010, it generated over 41% of the total global supply of palm oil [38]. Abdeljouad et al. [39] conducted an evaluation of POFA with the alkali activator potassium hydroxide (KOH) for stabilizing clayey soil. In addition, POFA utilized by Sukmak et al. [40] as a predecessor of POFA soft soil geopolymer, the alkaline activator employed in this study, consisted of a mixture of sodium hydroxide solution (NaOH) and sodium silicate solution (Na_2SiO_3). Moreover, the effect of utilizing POFA with a magnesium oxide activator as a laterite soil stabilizer as a replacement for OPC has been studied by Ezreig et al. [41]. Consequently, POFA reinforcement has been highlighted as a highly promising technique for enhancing soil characteristics in geotechnical engineering applications. In considering appropriate cases for numerical analysis, this study specifically focuses on OPC-stabilized and POFA-stabilized soil due to their significance in the soil stabilization field. This study emphasizes the capability of the concrete constitutive model to simulate the time-dependent behavior of stabilized soil due to pozzolanic reactions using traditional and non-traditional techniques. The structure of this article is organized as follows: The methodological

framework is presented in Section 2, and the experimental procedure is described in Section 3. Section 4 presents the experimental results and discussion. The numerical analysis is shown in Section 5, and this is followed by the numerical results and discussion in Section 6. Finally, the conclusion is presented in Section 7.

2. Methodological Framework

The methodology is comprised of two distinct phases. Phase 1 of the study primarily centers around conducting laboratory tests aimed at determining the index properties of the samples as well as performing engineering testing on the prepared specimens. Phase 2 involves the numerical analysis of two stabilized soil samples using 2D axisymmetric finite element analysis (FEA) with an advanced constitutive model. The methodological framework of this study is shown in Figure 1.
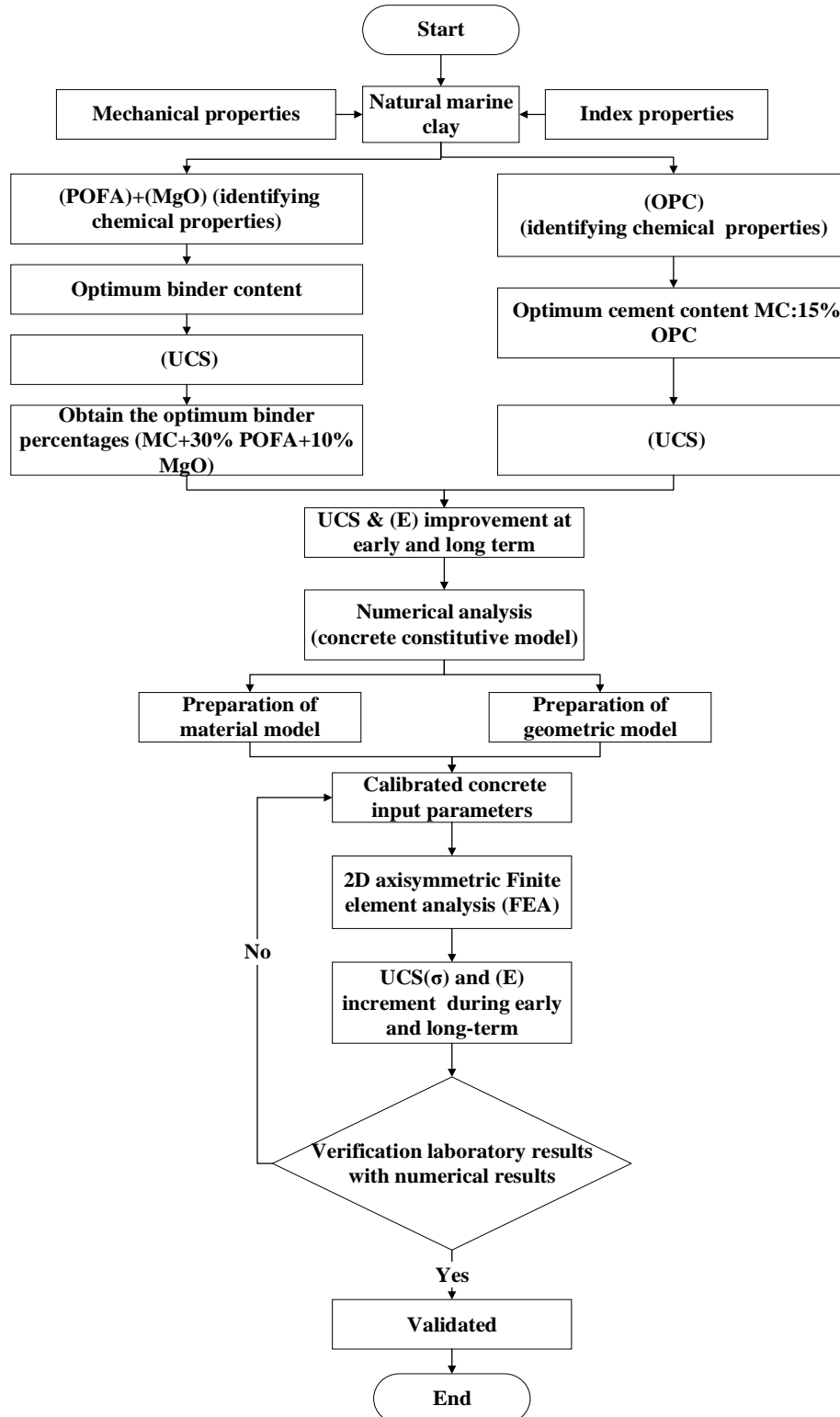

Figure 1. Methodology flowchart

3. Experimental Procedure

3.1. Soil Sample and Stabilizing Materials

The sample of marine clay was extracted from Nibong Tebal, Puala Penang, Malaysia, at a depth of 3 m from the ground surface. The investigated soil is mainly classified as inorganic silty clay with high plasticity (CH) according to the Unified Soil Classification System (USCS). The physical characteristics of the marine clay, in accordance with British Standards [42], are presented in Table 1. Ordinary Portland Cement (OPC) and Palm Oil Fuel Ash (POFA) were used as soil stabilizers for the numerical analysis. The oxide composition of OPC used in this study aligns with the chemical analysis used by Tsige et al. [12].

Table 1. Physical properties of marine clay

Soil properties	Quantity (%)
Specific gravity	2.56
Gravel content (%)	0
Sand content (%)	1.50
Silt content (%)	88.86
Clay content (%)	9.64
(MDD) (g/cm^3)	1.35
(OMC) (%)	29.8
Liquid limit (%)	62
Plasticity limit (%)	31
Plasticity index (%)	31

Palm oil fuel ash was sieved through a 300-micrometer sieve after drying for 24 hours at 105°C ± 5°C in an oven. According to the chemical analysis, POFA has a high silica (SiO_2) concentration, as indicated in Table 2. Nano MgO was used in this study as a chemical activator since it is an environmentally friendly and low-carbon soil stabilizer that leads to fewer CO_2 emissions [43, 44]. It might react with water rapidly because of its strong reactivity and low crystallinity. Figure 2 illustrates the utilized materials. The chemical composition of MgO utilized in this study is similar to the chemical analysis by Ezreig et al. [41]. Table 2 shows the chemical composition of the material used in this work.

Table 2. Chemical compositions of POFA and MgO

Oxides (%)	SiO_2	Al_2O_3	Fe_2O_3	CaO	MgO	K_2O	P_2O_5	SO_3	TiO_2	H_2O
POFA	49.5	2.18	12.30	17.61	-	8.42	9.52	0.70	0.61	-
MgO	-	-	0.01	-	99.5	-	-	0.03	-	0.02

Soft marine clay   **Nano Magnesium Oxide (MgO)**   **Palm Oil Fuel Ash (POFA)**

Figure 2. Utilized materials

3.2. Sample Preparation and Test Procedure

3.2.1. Soil-Binder Preparation

To decrease the water content, the marine clay samples were oven-dried at 105 °C for 24 hours after being collected. The materials were subsequently ground down, sieved, and passed through a sieve with 2 mm gaps. Deionized water was utilized throughout the process of preparing the samples. The first soil binder had 15% OPC (MC:15% OPC) [45, 46]. OPC is utilized herein as a reference stabilizer. The other was a mixture of soil with 40% of the binder by weight

of dry soil [41, 47, 48]. It was established with different mixtures of soil with POFA and MgO as activators (37.5% POFA+2.5%, 35% POFA+5% MgO, 32.5% POFA+7.5% MgO, and 30% POFA+10% MgO by weight of dry soil). Ezreig et al. [41] reported that the optimum binder content was 30% POFA:10% MgO.

3.2.2. Test Procedure (Unconfined Compressive Test)

To determine the axial stress-strain relationship, the UCS test was conducted. Moreover, this test aims to determine the optimum amount of stabilizing binder to apply to the considered marine clay in natural conditions before testing and analysis. The UCS tests were conducted under fixed conditions in accordance with the D2166_D2166M-16 [49]. Three cylindrical samples were examined for compressive strength. Each sample that performed the UCS test was cured for one, three, seven, 14, and 28 days, respectively. The samples were compressed at a constant rate of 1 mm/minute until failure, as shown in Figure 3.

Figure 3. Prepared samples for the unconfined compression test

4. Experimental Results and Discussion

Three types of soil, including 1) natural marine clay, 2) clay mixed with OPC, and 3) clay mixed with POFA and MgO, were used in the UCS test to determine the effectiveness of the additive in enhancing compressive strength. The UCS and curing time of the mixtures NMC MC-B40 were plotted, as shown in Figure 4. The stabilized soil samples with 30% POFA-10% MgO gave the highest UCS development among the mixtures at seven and 28 days of curing, respectively. The stress-strain behavior of the stabilized samples with the optimum content of both stabilizers is presented in Figure 5. It is evident that, initially, the stress grows slowly before rapidly increasing with a specific strain until it reaches its peak stress. Afterwards, the stress declined for both stabilized soils [50]. This also shows that the post-failure stress of stabilized soil drops much more rapidly with a longer curing period than with a shorter curing period [51]. As shown in Figure 5, there are significant increases in the UCS of all stabilized samples with an increasing curing period, and this has been reported by many researchers [52–55]. The results show that the strength increased from 257 kPa for untreated soil to 2270 kPa and 2881 kPa for soil with 15% OPC at seven and 28 days, respectively.
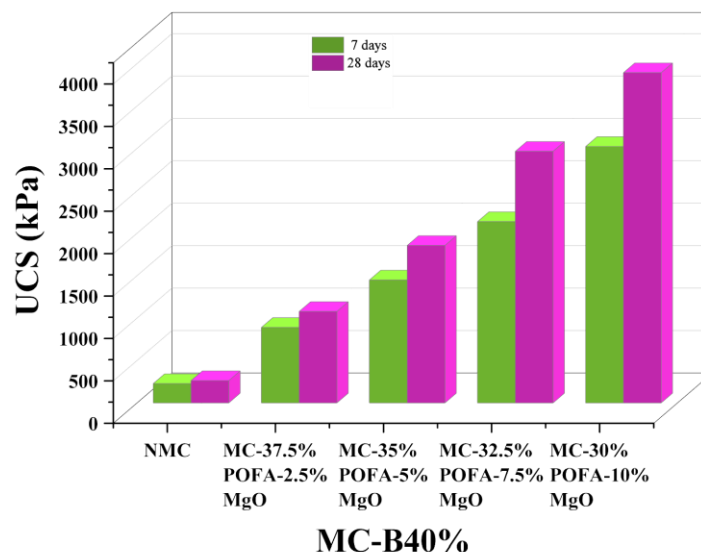

Figure 4. Test results of compressive strength at seven and 28 days of curing for stabilized samples with different doses of the binder
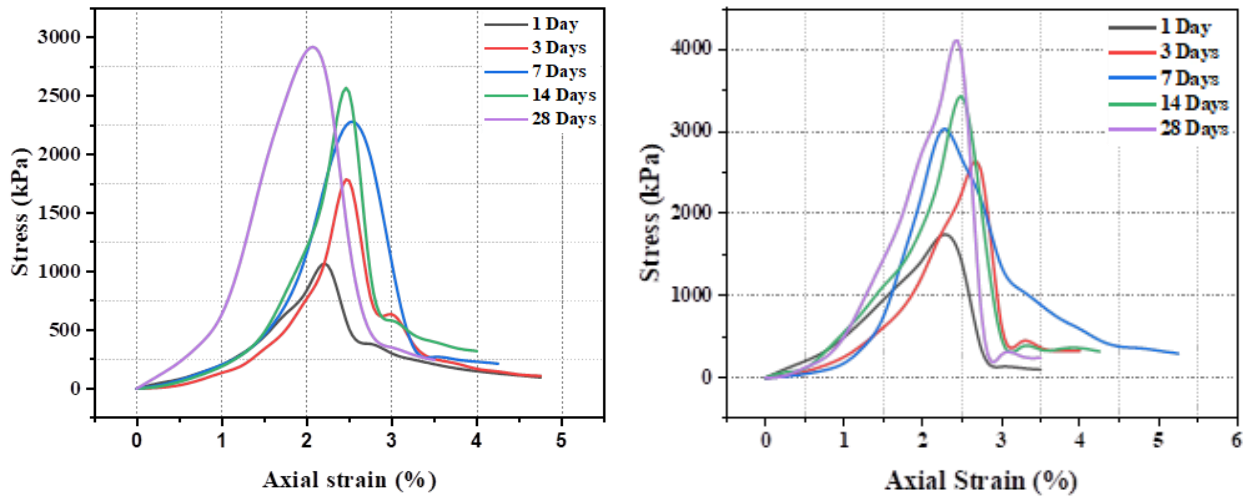
Figure 5. Axial stress vs. strain for (a) MC: 15% OPC and (b) MC: 30%POFA:10%MgO

Several studies also reported increased strength with cement concentration for a given curing time [56-59]. The improvement in strength during the 28-day curing period was caused by the cement's hydration process, resulting in the production of Calcium Silicate Hydrate (C-S-H) and Calcium Aluminate Hydrate (C-A-H) [60, 61]. C-S-H and C-A-H, by cement hydration, can bind rapidly with clay particles. This increases cohesion and strength by filling the spaces between soil particles. The concentration of hydroxyl ions (OH-) in the soil-binder combination rises as the curing time increases. This raises pH and causes ions from silica and alumina compounds to dissolve in the clay particles, thereby improving OPC hydration [62].

Moreover, it can be noticed that the rate of increasing strength is high during the three days of curing and that 61.5% of maximum strength was achieved at 28 days. This can be explained as early-age strength development that is mainly dependent on cement hydration and cementitious compound production [56]. The consumption of the available cement and a reduced reaction rate lead the rate of strength development to decrease over time [62]. For POFA-stabilized soil, it was shown that the UCS increased from 257 Kpa for untreated soil to 3023 kPa and 3894 kPa for treated soil with 30% POFA-10% MgO at seven and 28 days, respectively, as seen in Figure 6b. The flocculation of soil particles due to the cation exchange process is related to the increased stabilized soil strength during a shorter curing period [63]. As a result of the interaction between nanoparticles and soil during a longer curing period, cementing gels, including magnesium silicate hydrate (M-S-H) and magnesium aluminate hydrate (M-A-H), and others, were formed, improving the binding of the soil particles and enhancing the UCS of the treated soil.
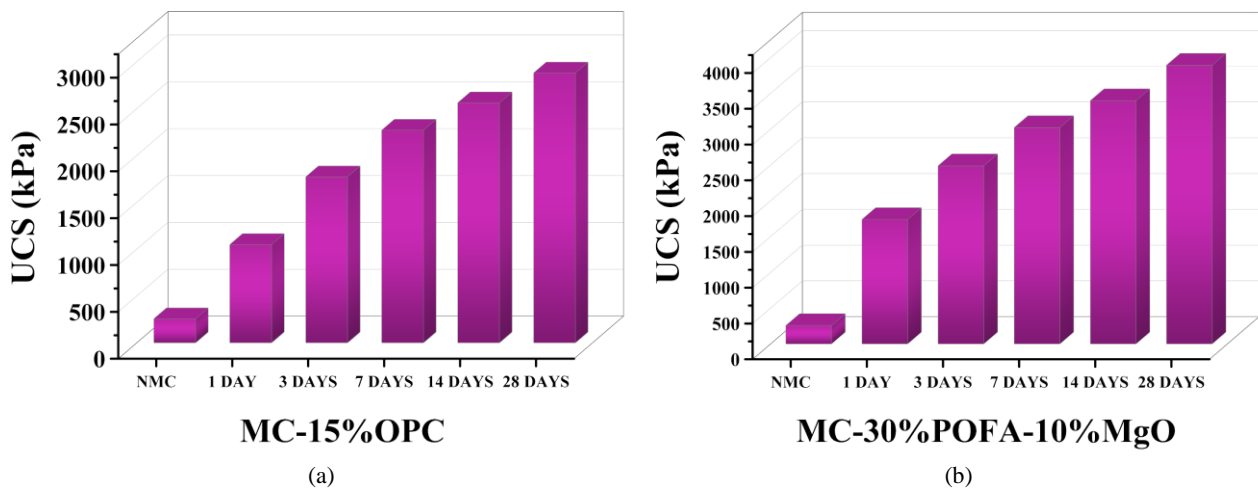

(a)

(b)

Figure 6. Unconfined compressive strength of (a) MC-15% OPC and (b) MC-30%POFA-10%MgO at different curing periods

The second mechanism is the pozzolanic reaction, which further produces magnesium aluminate silicate hydrate gel. This occurs when magnesium and silica react with aluminium present in the precursor (POFA) [41, 64]. It was demonstrated that the Mg interaction is time-dependent and that the bonding of soil particles with POFA-based MgO develops over time. In fact, the UCS of MC after seven and 28 days of curing were superior to the UCS reported by Khasib et al. [47], who performed investigations on the high-plasticity marine clay treated with POFA as source material and NaOH along with Na_2SiO_3 as alkali activators. This achieved 1000 kPa and 2800 kPa at seven and 28 days,

respectively. Compared with OPC-stabilized soil, the strength of all POFA-stabilized samples generally increases more than the strength of OPC-stabilized samples. The percentage gain in maximum stress between soil stabilized by OPC and soil stabilized by POFA is about 33% and 35% at seven and 28 days of curing, respectively.

5. Numerical Analysis

5.1. Modelling Details

PLAXIS 2D has been used to analyze the behavior of stabilized soil. This is finite element software for geotechnical applications in which soil models simulate deformation, stability, and water flow in geotechnical engineering. It can use finite element methods to solve the imbalance caused by geotechnical works such as raising dams and embankments, flooding, and removing soil for excavation geotechnics. It also solves the stress-strain relationships using constitutive soil models. This research utilized the concrete model to simulate OPC-stabilized and POFA-stabilized soil behavior.

5.2. Finite Element Mesh, Boundary Conditions, and Analysis Procedure

Creating a finite element model using PLAXIS begins with a geometry model. The model was assigned physical and mechanical properties to calculate the behavior of the stabilized soil. Due to the cylindrical shape of the samples, the model will be chosen in PLAXIS, an axisymmetric model with 25 mm width and 100 mm height. It is assumed that the strain is the same in all directions. The general properties of the two samples are shown in Table 3. The 15-node triangular components were employed to discretize the entire soil domain; a similar approach has been used in the literature. This demonstrates a fourth-order interpolation for displacements with the numerical integration including 12 Gauss points (stress points), providing more accurate modeling of curvature, complex behavior, and stress concentrations [65]. A very fine mesh is used to enhance the accuracy of the analysis. Figures 7 and 8 show the geometry of the model and the finite element mesh for both samples. The boundary is fully fixed at Xmin and Ymin to the bottom for the boundary conditions. Therefore, there are no motions in vertical directions to the symmetry lines.

Table 3. General properties of stabilized marine clay

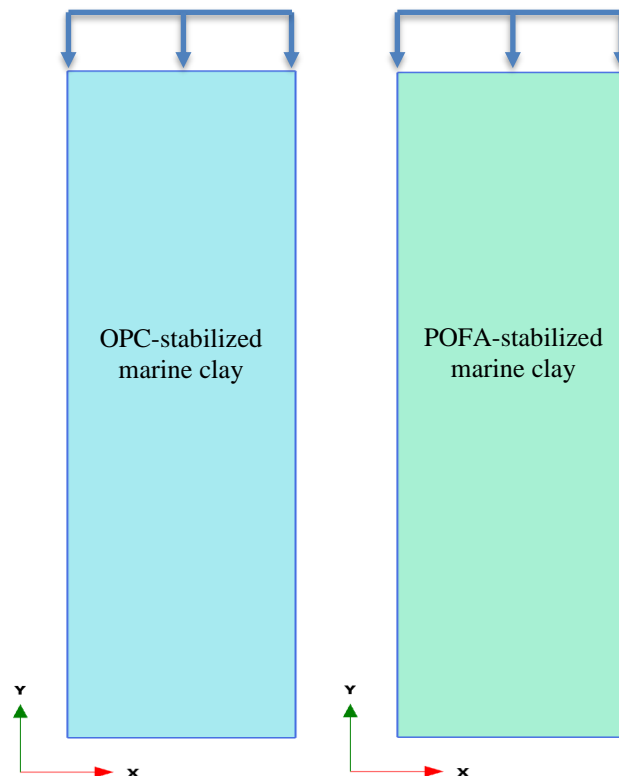| Properties	MC-OPC	MC-POFA-MgO
Soil condition	Drained	Drained
γ_{unsat} (Kn/m^3)	16.5	19.1
γ_{sat} (Kn/m^3)	22.44	25.8
Initial void ratio	0.99	1.04

Figure 7. Geometry model of (a) OPC-stabilized soil and (b) POFA-stabilized soil
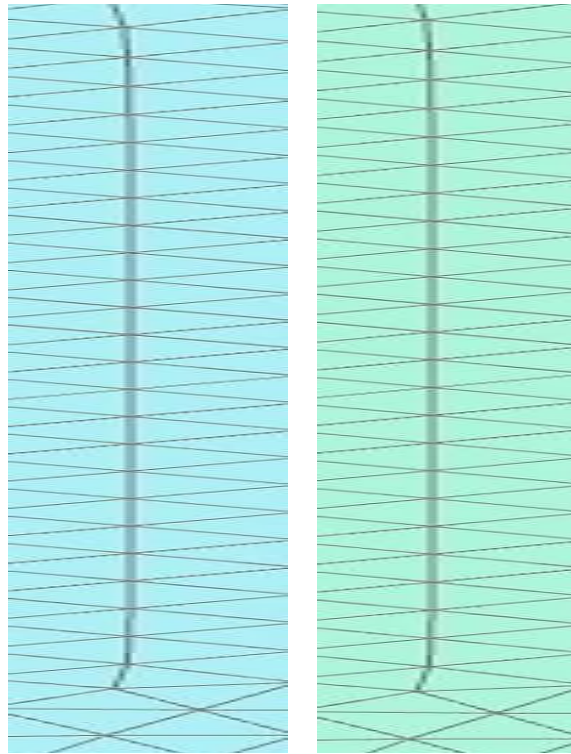
Figure 8. Mesh of model geometry of (a) OPC-stabilized soil and (b) POFA-stabilized soil

5.3. Constitutive Model and Model Parameters

An appropriate constitutive model must be utilized during the numerical analysis to represent the behavior of the soil accurately. This work simulates stabilized soil behavior using a concrete constitutive model built in PLAXIS 2D software. This is an elastoplastic model for modeling concrete's time-dependent stiffness, strength, creep, shrinkage, and strain hardening-softening in compression and tension. Also, it considers the non-linear behavior of the material. It was initially created to simulate the behavior of shotcrete but is also effective for soil improvement, for example, with jet grout columns. In the shotcrete model, the development of stiffness with time complies with the recommendation of the CEB-FIP model code [66–72]:

$$E(t) = E_{28} \, e^{S \, stiff \, \left(1 - \sqrt{\frac{28}{t}}\right)}$$
(1)

while E_{28} is Elastic modulus at 28 days, E_1 is Elastic modulus at 1 day, S_{stiff} is related to the stiffness ratio at 1 day and t_{hyd}, E_1/E_{28}, as in Equation 2. Furthermore, the (S_{stiff}) parameter controls the variation of stiffness with time.

$$S_{stiff} = -\frac{\ln(E_1/E_{28})}{\sqrt{28}-1}$$
(2)

As with the improvement of Young's modulus, the development of unconfined compression strength with time is described following the recommendation of the CEB-FIP model code:

$$F_{cu}(t) = f_{cu}^{(28)} \exp\left(S_{strength}\left(1 - \sqrt{28/t}\right)\right)$$
(3)

where $F_{c,28}$ is UCS at 28 days, $F_{c,1}$ is UCS at 1 day, $S_{strength}$ is related to the stiffness ratio at 1 day and t_{hyd}, $F_{c,28}/F_{c,1}$, as in Equation 4. Furthermore, the $S_{strength}$ parameter controls the variation of the strength with time.

$$S_{strength} = \frac{-\ln(F_{cu}^{(1)}/F_{cu}^{(28)})}{\sqrt{28}-1}$$
(4)

In the shotcrete model, the improvement of ductility material is described by the reduction of uniaxial plastic failure strain with time (ε^p_{cpu}) by determining the values of (ε^p_{cpu}) at the period of 1 h, 8 h and 24 h, $\varepsilon^p_{(1)cpu}$, $\varepsilon^p_{(8)cpu}$ and $\varepsilon^p_{(24)cpu}$.

5.4. Concrete Model Calibration and Parameter Determination

Since it is costly and time-consuming to test soil in a laboratory in its early stages of curing, finding high-quality test results in the literature can be challenging. Experimental work focuses mainly on the negligible unconfined compression strength during curing. It is shown below that the proposed constitutive model can represent stabilized soil's stress-strain behavior, including failure behavior.

To calibrate the parameters utilized in the analysis, the unconfined compressive test is simulated numerically with concrete constitutive models using a soil-test facility. Calibrated parameters for OPC-stabilized marine clay and POFA-stabilized marine clay are listed in Tables 4 and 5. Figures 9 and 10 illustrate the axial stress-strain curves from the test and simulation. It should be mentioned that the failure behavior can be captured by a concrete model, similar to a study conducted by Waichita et al. [25].

Table 4. Calibrated parameters of a concrete constitutive model for OPC-stabilized marine clay

Parameter	Value	Reference
E_{28}	170000 kPa	Calibrated from PLAXIS soil test
N	0.25	Recommended by Waichita et al. [25]
$f_{c,28}$	3000 kPa	Calibrated from PLAXIS soil test
f_{c0n}	0.1	Calibrated from PLAXIS soil test
f_{cfn}	0.5	Calibrated from PLAXIS soil test
f_{cun}	0.1	Calibrated from PLAXIS soil test
$Gc_{,28}$	28 kn/m	Calibrated from PLAXIS soil test
$\emptyset_{max}$	40	Recommended by Yapage & Liyanapathirana [68]
ψ	0	Recommended by Ong & Tan [26], Shaalan et al. [22]
$f_{t,28}$	317 kPa	Lab test ($f_{t,28} = 0.11\ f_{c,28}$)
f_{tun}	0	Recommended by Maatkamp [28], Waichita et al. [25], Wahab et al. [61]
$G_{t,28}$	0.01 kn/m	Recommended by Waichita et al. [25]
E_1/E_{28}	0.50	Calibrated from PLAXIS soil test
$f_{c,1}/f_{c,28}$	0.36	Calibrated from PLAXIS soil test
a_{duct}	16	Recommended by Ong & Tan [26]
$\varepsilon^P_{(1)\,cp}$	-0.05	PLAXIS (2022) [66]
$\varepsilon^P_{(8)\,cp}$	-0.0015	PLAXIS (2022) [66]
$\varepsilon^P_{(24)\,cp}$	-0.0012	PLAXIS (2022) [66]
t_{hyd}	28	

Table 5. Calibrated parameters of a concrete constitutive model for POFA-stabilized marine clay

| Parameter	Value	Reference
E_{28}	182000 kPa	Calibrated from PLAXIS soil test
N	0.35	Recommended by Yaro et al. [70]
$f_{c,28}$	4000 kPa	Calibrated from PLAXIS soil test
f_{c0n}	1	Calibrated from PLAXIS soil test
f_{cfn}	0.5	Calibrated from PLAXIS soil test
f_{cun}	0.1	Calibrated from PLAXIS soil test
$Gc_{,28}$	38 kn/m	Calibrated from PLAXIS soil test
$\emptyset_{max}$	18	Recommended by Khasib et al. [47]
ψ	0	Recommended by Ong & Tan [26]
$f_{t,28}$	438.35 kPa	Lab test ($f_{t,28} = 0.11\ f_{c,28}$)
f_{tun}	0	Recommended by Maatkamp [28], Waichita et al. [28], Vinoth et al. [69]
$G_{t,28}$	0.01 kn/m	Recommended by Waichita et al. [25]
E_1/E_{28}	0.5	Calibrated from PLAXIS soil test
$f_{c,1}/f_{c,28}$	0.46	Calibrated from PLAXIS soil test
a_{duct}	16	Recommended by Ong & Tan [26]
$\varepsilon^P_{(1)cp}$	-0.01	PLAXIS (2022) [66]
$\varepsilon^P_{(8)cp}$	-0.0015	PLAXIS (2022) [66]
$\varepsilon^P_{(24)cp}$	-0.00022	Calibrated from PLAXIS soil test
t_{hyd}	28	
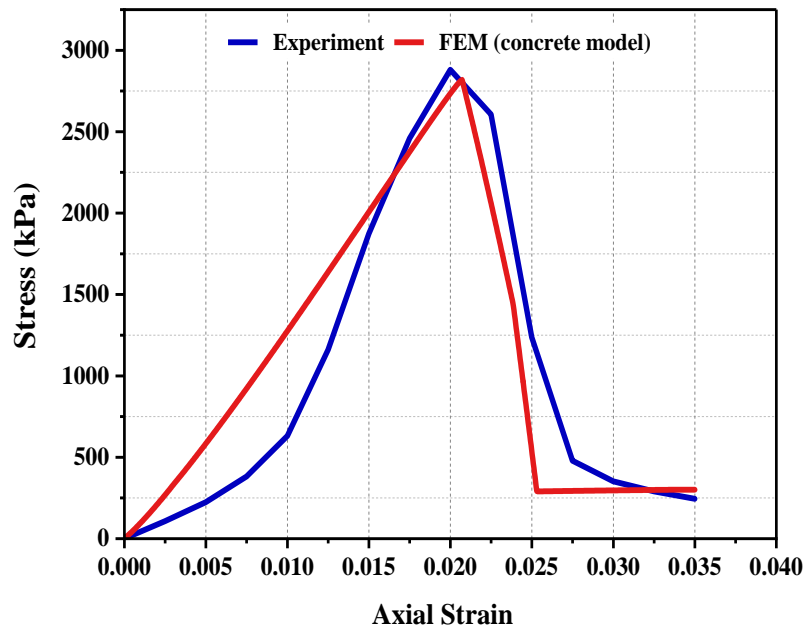
Figure 9. Axial stress-strain result of the unconfined compressive test on OPC-stabilized marine clay with the simulation results of the concrete model
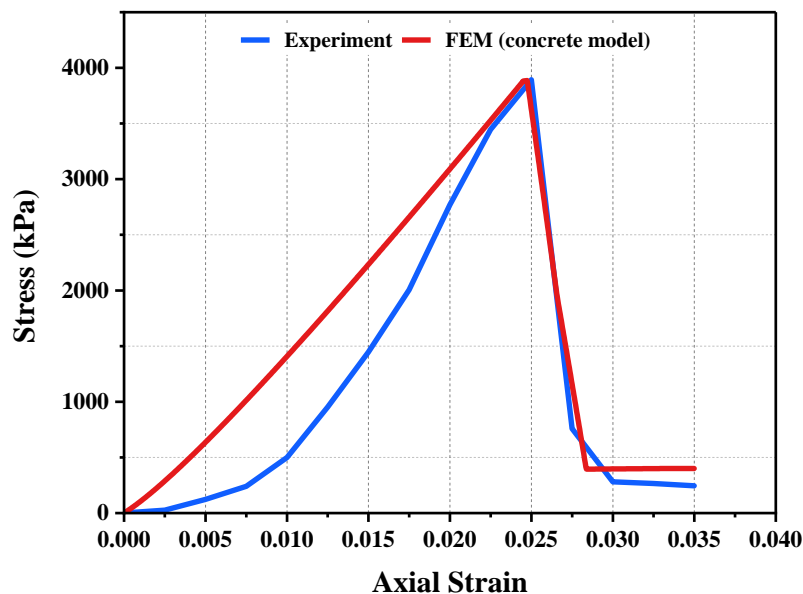

Figure 10. Axial stress-strain result of the unconfined compressive test on POFA-stabilized marine clay with the simulation results of the concrete model

6. Results and Discussion

## 6.1. Parameter Sensitivity Analysis

A sensitivity analysis is carried out to investigate the concrete model parameters' influence on stabilized soil's stress-strain behavior. This involves deactivating the model parameters separately and evaluating their effect on the stress-strain relationship. The soil-test facility is utilized to achieve the parameter sensitivity analysis. According to previous modeling by Maatkamp [28], a general soil test simulates an unconfined compression test. The parameters with the most influence on the stress-strain curve are evaluated, and this was done on a POFA-stabilized soil sample.

6.1.1. Elastic Modulus (*E*28)

The elastic modulus, at 28 days of curing, can be calculated from the stress-strain curve obtained from laboratory tests at 28 days.

Table 4. Elastic modulus (E_{28}) sensitivity analysis cases (the increments between (0-3) cases seem to be 20E+3 kPa)

Parameter	Values (kPa)	Case	References
E_{28}	110E+3	0	Reference
E_{28}	130E+3	1	
E_{28}	150E+3	2	
E_{28}	170E+3	3	
E_{28}	182E+3	4	Calibrated from PLAXIS soil test
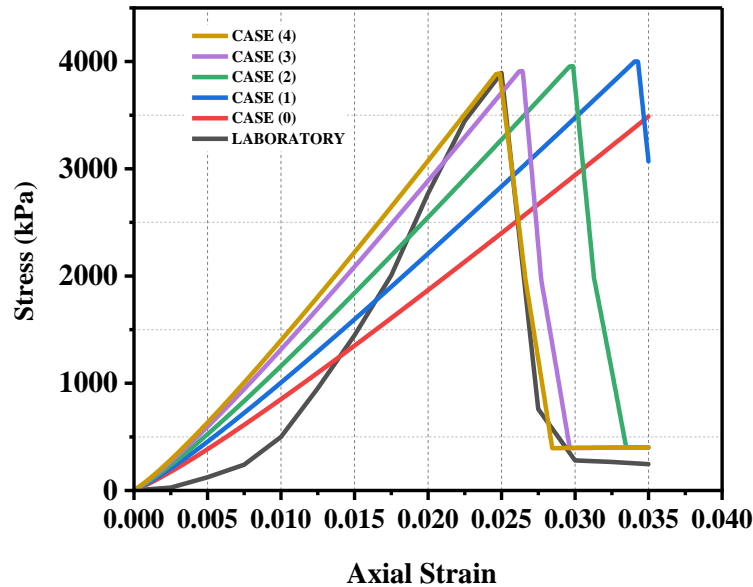
Figure 11. The model sensitivity to (E_{28}) in a stress-strain curve by cases (0-4)

As shown in Figure 11, the stress-strain curve is noticeably affected by the increase in the elastic modulus, with failure strain occurring earlier in the loading process. Soils with a higher elastic modulus are less likely to deform significantly before the failure point. Compared to soils with lower elastic modulus, this trend shows increased material stiffness and improved resistance to deformation since strain starts to occur at lower stress levels [73–76]. As the elastic modulus of the stabilized soil increases, the stress-strain curve undergoes a significant change from a linear elastic behavior to a linear elastic-brittle failure behavior.

6.2.1. Time-Dependent Stiffness-Strength Parameters

Time-dependent parameters include the hardening of the soil with curing time. The parameters under consideration are E_1/E_{28} and fc_1/fc_{28}. The parameter sensitivity is evaluated according to the cases given in Tables 7 and 8.

Table 5. Time-dependent stiffness sensitivity analysis cases

Parameter	Value	Case	Reference
E_1/E_{28}	0.4	43	
E_1/E_{28}	0.5	44	
E_1/E_{28}	0.65	45	Calibrated from PLAXIS
E_1/E_{28}	0.8	46	soil test [22]
E_1/E_{28}	1	47	

Table 6. Time-dependent strength sensitivity analysis cases

Parameters	Values	Cases	References
fc_1/fc_{28}	0.25	48	
fc_1/fc_{28}	0.46	49	Calibrated from PLAXIS
fc_1/fc_{28}	0.8	50	soil test [22]
fc_1/fc_{28}	1	51	

The results of applying the cases (43–47) given in Table 7 are visualized in Figure 12, considering stress-strain behavior. The lines in the graph are divided in the order of the cases in which they are illustrated.
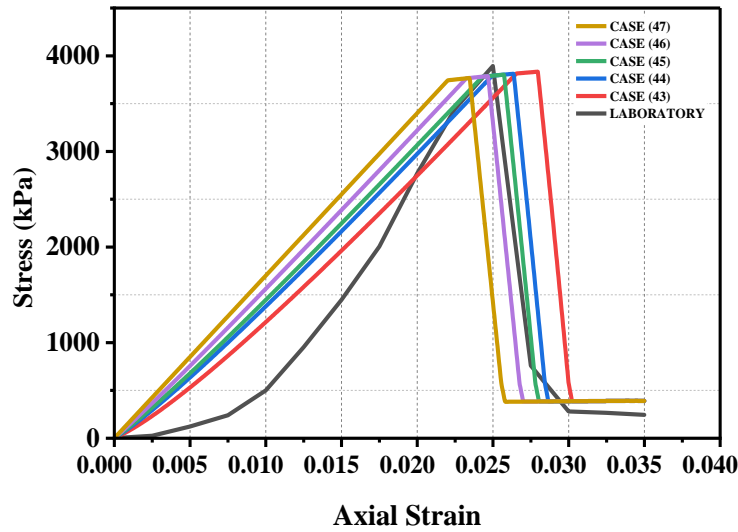

Figure 12. The model sensitivity to (E_1/E_{28}) in a stress-strain curve by cases (43-47)

The slope of the stress-strain curve becomes more gradual when the stiffness ratio between days one and 28 decreases, and this also affects the tangent of the curve. Therefore, as the ratio decreases, it exhibits more deformation under stress, resulting in a decreasing slope on the stress-strain curve. Nevertheless, the generation of failure strain will be delayed. This effect aligns with the investigation reported by Maatkamp [28].

The cases for the fc_1/fc_{28} sensitivity analysis are presented in Table 8. The results of applying the different cases in the unconfined compression test are presented in Figure 13. The failure stress that the material experiences decrease slightly as the strength ratio decreases. Moreover, as the fc_1/fc_{28} decreases, the failure strain is generated earlier. Although this parameter affects the stress-strain curve, its impact is considered relatively insignificant. Despite the differences between the materials used and their behavior in this study and those in the study conducted by Maatkamp [28] on the concrete structure, both show the same effect on the stress-strain curve, taking into consideration that the effect in Maatkamp [28] is more significant than in our study.
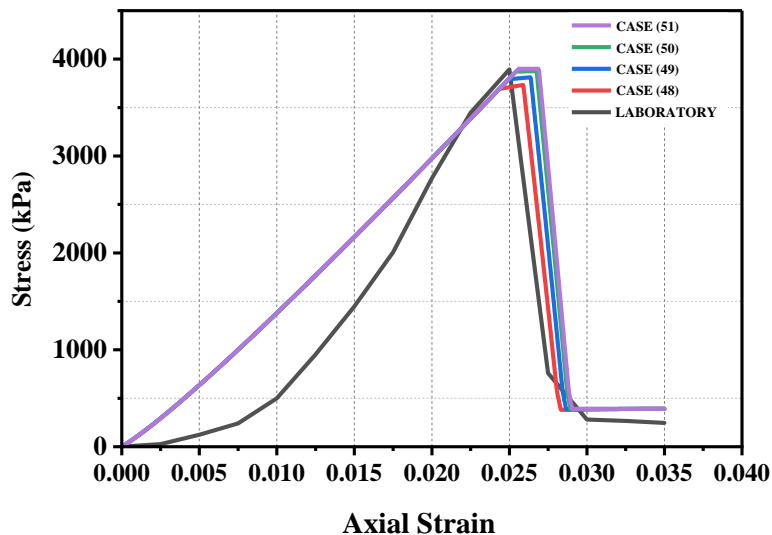

Figure 13. The model sensitivity to (fc_1/fc_{28}) in a stress-strain curve by cases (48-51)

6.2. UCS (σ) Improvement

A precise analysis and estimation of strength and stiffness improvement over time are produced by FEM. The effect of OPC and POFA on the early strength and stiffness of the soil was studied numerically using a concrete model. Figure 14 illustrates the increment of UCS with time for both stabilized soil samples.
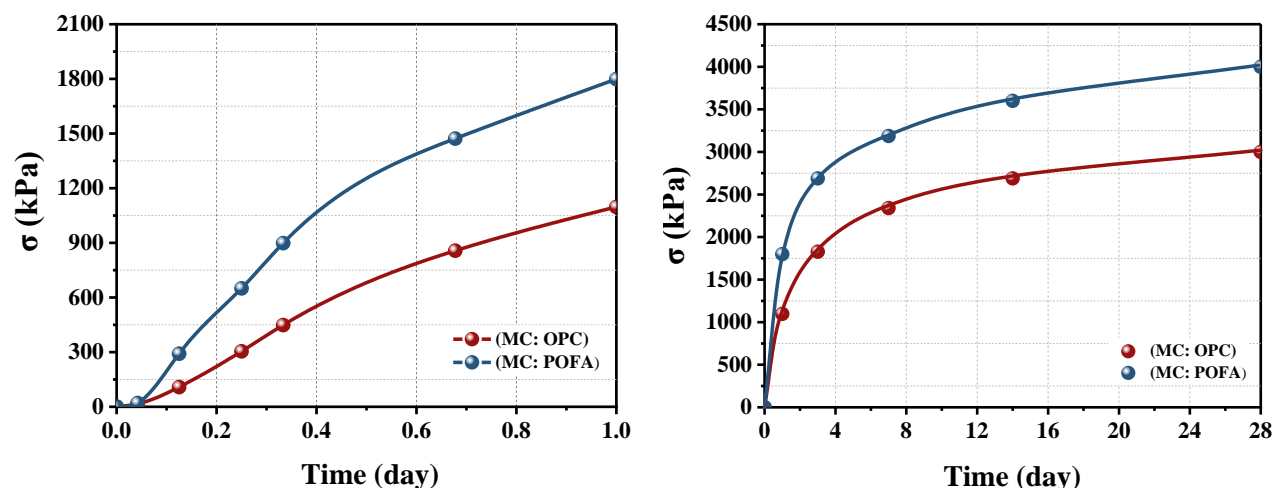
Figure 14. Increment of the unconfined compressive strength of stabilized marine clay at (a) short term (one day) and (b) long term (28 days): numerical results based on the calibrated concrete model

Anticipating the above figure shows that POFA-stabilized soil exhibits a more rapid early-age strength gain compared with OPC-stabilized soil. It also demonstrates a substantial rise in strength compared with OPC-stabilized soil, with 64.02% and 47% after one day and three days, respectively. It can also be noted that the greater growth rate was after three days of curing for both stabilized soil samples. The strength reached 70% and 69% of the maximum strength by 28 days for (MC: OPC) and (MC: POFA), respectively. This is a higher growth rate than in the results reported by N. Jiang et al. [50]. These results demonstrate that POFA will be a more efficient early-age strength enhancer than OPC, indicating that POFA can be an effective alternative stabilizer for soil.

As a precursor, POFA, which is rich in reactive Al and Si ions in the presence of MgO, significantly impacted the increase of UCS by producing Al-O-Si and Si-O-Si chains, resulting in a strong and dense soil mixture [48]. While MC: OPC achieved 2340 kPa and 3000 kPa, MC: POFA reached 3187 kPa and 4000 kPa at seven and 28 days, respectively. Notably, clay soil's strength improved by approximately 36% and 33% with optimum POFA content, compared with OPC content, at seven and 28 days, respectively. Showing a substantial gain over OPC-stabilized clay after 28 days. The comparison of UCS values between OPC-stabilized soil and POFA-stabilized soil is shown in Table 9. This indicates the potential effectiveness of this technique in practical application in deep soil mixing construction. Moreover, utilizing POFA as a precursor demonstrates a promising technique in geotechnical engineering applications such as subgrade and sub-base materials for road construction and foundation elements [77].

Table 7. Comparison of UCS values between OPC-stabilized soil and POFA-stabilized soil

Curing times (days)	UCS values for OPC-stabilized soil (kPa)	UCS values for POFA-stabilized soil (kPa)	Growth rate (%)
1 day	1097	1799	+64.02
3 days	1827	2689	+47
7 days	2340	3187	+36
28 days	3000	4000	+33

6.3. Stiffness (E) Improvement

In the second part of the study, the proposed model can estimate the time-dependent stiffness of stabilized soil even in the early stages of curing. The stiffness variation when adding POFA to marine clay will be analyzed and compared with OPC-stabilized marine clay in particular. It can be observed that significant improvement was obtained. As shown in Figure 15, the elastic modulus rapidly increased during 24 hours of curing. It achieved approximately 50% and 53% of the maximum stiffness at 28 days of curing for (MC: OPC) and (MC: POFA), respectively, demonstrating a significant rise in stiffness. Regarding time-dependent stiffness, the results obtained in the current study are higher than those proposed by Mahvash-Mohammadi [78]. It appears, from a comparison of each of the stabilizers, that the addition of POFA has resulted in a significant increase in the early stiffness of the soil.
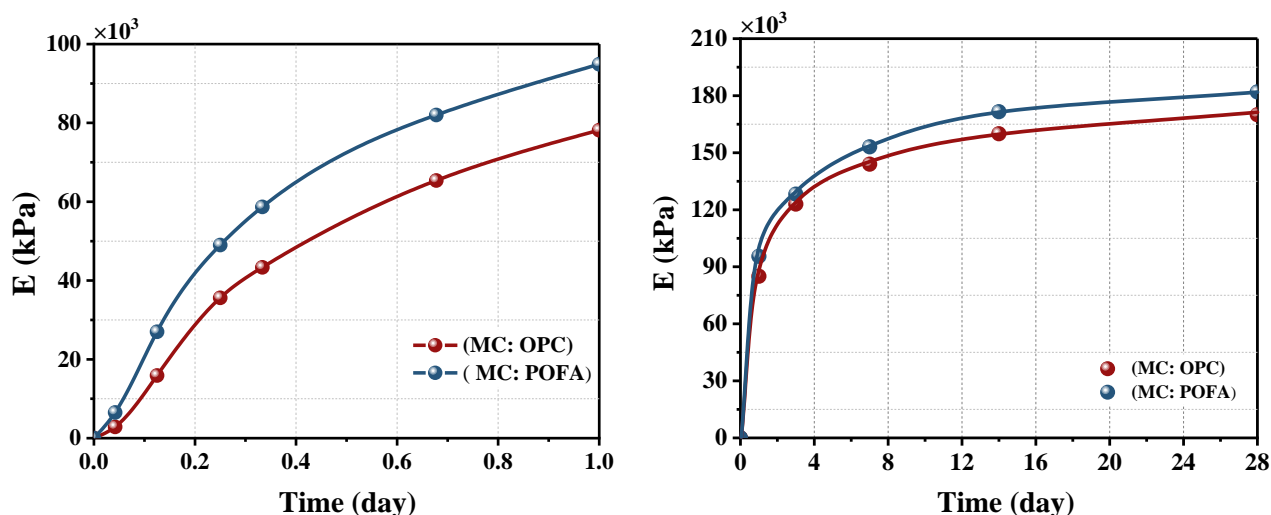
Figure 15. Increment of elastic modulus of stabilized marine clay at (a) short term (one day) and (b) long term (28 days): numerical results based on the calibrated concrete model

During the early curing stages, the pozzolanic reaction is very rapid, leading to early stiffness gain in stabilized soil. It is evident from Figure 15 that both materials show similar trends in the development of stiffness with time. The percentage gain in stiffness between the soil stabilized by OPC and the soil stabilized by POFA is around 6% and 8% at seven and 28 days of curing, respectively. However, it should be noted that the rate of increase in stiffness of the POFA-stabilized soil is higher than that of the OPC-stabilized soil during the early age of curing. The comparison of elastic modulus values between OPC-stabilized soil and POFA-stabilized soil is shown in Table 10.

Table 8. Comparison of elastic modulus values between OPC-stabilized soil and POFA-stabilized soil

Curing times (days)	(E) values of OPC-stabilized soil (kPa)	(E) values of POFA-stabilized soil (kPa)	Growth rate (%)
1 day	85000	95480	+12.34
3 days	123000	128200	+4.23
7 days	144000	153100	+6
28 days	170000	182000	+7

6.4. Concrete Model Validation

In order to demonstrate the applicability of the concrete model to simulating the time-dependent behavior of stabilized soil, the strength and stiffness values are determined at different curing periods and then compared with the simulated results.

6.4.1. Time-Dependent Strength (σ)

The comparison between the concrete model results and the laboratory results is presented in Figure 15, in which the improvement of the UCS (σ) of the stabilized soil samples with time is evaluated at different curing periods. The results demonstrate a good agreement between predicted and experimental results for OPC-stabilized soil. While the Finite Element Method (FEM) yields strength values slightly higher than the laboratory results, the difference is considered insignificant, with variations of 4.47%, 3.057%, 3.04%, 6.24%, and 4.05% at different curing times, as shown in Table 11. On the other hand, for POFA-stabilized marine clay, the comparison shows a good quantitative agreement between the predicted and measured results, with variations of 3.39%, 7.73%, 5.28%, 5.744%, and 2.685% at different curing times, as shown in Table 12. This demonstrates the concrete model's capability in predicting the stabilized soil's time-dependent strength, considering that the concrete model takes only 28 days into account. The analysis results and comparisons between this model and the laboratory results of concrete compressive strength improvement of tunnel lining with time show a good agreement for 28 days [79].

Table 9. Comparison between experiment and numerical results of UCS of (OPC-stabilized soil)

Curing times (days)	Experiment results (kPa)	Numerical results (kPa)	Variations (%)
1 day	1049	1097	4.47
3 days	1772	1827	3.057
7 days	2270	2340	3.04
14 days	2526	2689	6.24
28 days	2881	3000	4.05

Table 10. Comparison between experiment and numerical results of UCS of (POFA-stabilized soil)

Curing times (days)	Experiment results (kPa)	Numerical results (kPa)	Variations (%)
1 day	1739	1799	3.39
3 days	2489	2689	7.73
7 days	3023	3187	5.28
14 days	3399	3600	5.74
28 days	3894	4000	2.69

6.4.2. Time-Dependent Stiffness (E)

Figure 16 shows the comparison between the predicted and measured stiffness improvements of both stabilized soil samples. The numerical analysis results exhibit a precise estimation of stiffness improvement during the 28 days of curing for OPC-stabilized soil, with variations of 7.59%, 11.60%, 1.41%, 3.36%, and 0.47% at different curing times, as shown in Table 13. For POFA-stabilized soil, the stiffness values align closely with the corresponding laboratory test results, with variations of 0.82%, 6.47%, 4.73%, 10.56%, and 0.44% at different curing times, as shown in Table 14. This aligns with the findings of a study conducted by Shaalan et al. [80]. Which proved the applicability of the proposed model with shotcrete lining time-dependent stiffness estimation.
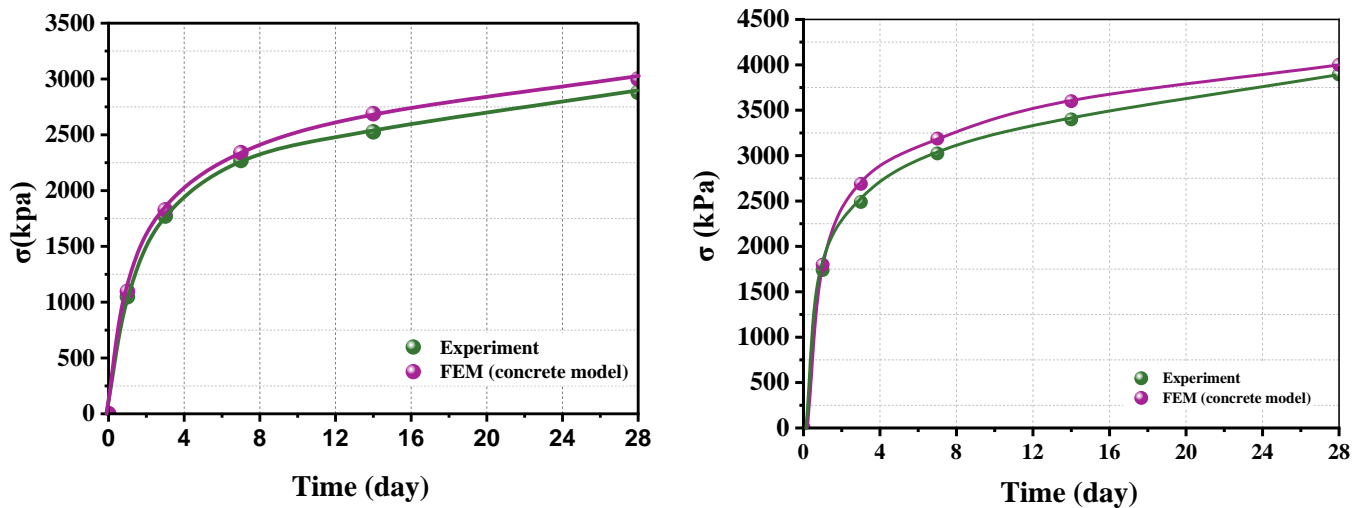

Figure 16. Concrete model validation for compressive strength development with time of (a) OPC-stabilized soil and (b) POFA-stabilized soil

Table 11. Comparison between experiment and numerical results of (E) of (OPC-stabilized soil)

Curing times (days)	Experiment results (kPa)	Numerical results (kPa)	Variations (%)
1 day	79000	85000	7.59
3 days	100300	123000	22.57
7 days	142000	144000	1.41
14 days	154800	160000	3.36
28 days	169200	170000	0.47

Table 12. Comparison between experiment and numerical results of (E) of (POFA-stabilized soil)

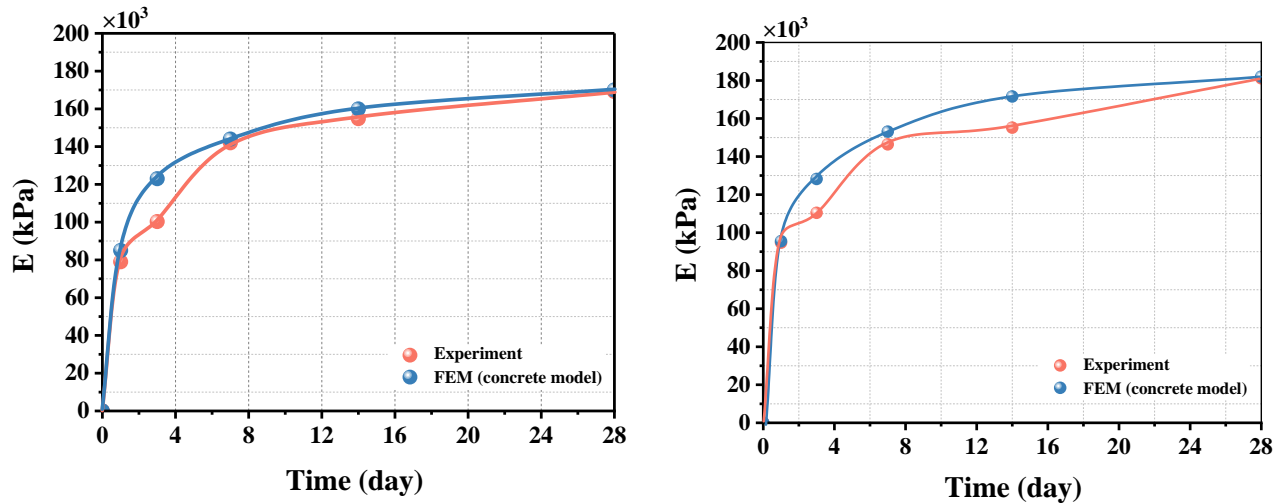| Curing times (days)	Experiment results (kPa)	Numerical results (kPa)	Variations (%)
1 day	94700	95480	0.82
3 days	110400	128200	16.14
7 days	146400	153100	4.73
14 days	147200	171600	16.56
28 days	181200	182000	0.44

Figure 17. Concrete model validation for stiffness development with time of (a) OPC-stabilized soil and (b) POFA-stabilized soil

7. Conclusion

In the present study, POFA-stabilized soil was investigated numerically as a replacement for OPC-stabilized soil with finite element analysis, PLAXIS 2D. The concrete model was used to simulate time-dependent strength and stiffness improvements. Depending on the experimental results, the calibration of model parameters was achieved. A parameter sensitivity analysis was performed to study the effect of each parameter on the stress-strain curve, and the parameters with the greatest effect were then illustrated.

The main findings of this study include a noticeable improvement in the Unconfined Compressive Strength (UCS) of POFA-stabilized soil. It increases rapidly at the early age of curing within the optimum binder content. It also exhibits more rapid early-age strength gain compared with cement-stabilized soil. The highest UCS growth rate reached 64% during the first three days of curing at optimum binder content. After three days, the growth rate slowed. This can be attributed to the gradual consumption of magnesium oxide, an essential component of pozzolanic reactions. According to the calibration, the concrete constitutive model is valuable for comprehensively understanding the mechanism involved in the stabilization process, enabling a more accurate representation of stress-strain behavior. It can be noticed that the stress-strain curve obtained from the proposed model aligns with the stress-strain curve obtained from the laboratory results. It exhibits a notable ability to capture the failure behavior of stabilized soil. According to parameter sensitivity analysis, the elastic modulus (E_{28}) and time-dependent stiffness parameter (E_1/E_{28}) influence the stress-strain behavior most. Higher elastic modulus accelerates the failure strain occurring in the stress-strain curve, indicating greater material stiffness and resistance to deformation compared with lower-modulus soils. As the stiffness ratio between days one and 28 decreases, the stress-strain curve exhibits a more gradual slope, leading to increased deformation under stress and a delayed generation of failure strain.

Based on the numerical results, the early strength of POFA-stabilized soil demonstrated a 47% and 64.02% increase in UCS values at one and three days, respectively, compared with OPC-stabilized soil. Meanwhile, compared with OPC, it also exhibited significant improvement by approximately 36% and 33% with optimum content at seven and 28 days, respectively. For stiffness development, POFA-stabilized soil significantly increased early stiffness compared with OPC-stabilized soil. On the other hand, the increment rate of POFA-stabilized soil reached 7% and 8% in seven and 28 days, respectively, compared with OPC-stabilized soil. Comparing the UCS and stiffness values obtained from the stress-strain curves after one, three, seven, 14, and 28 days in the laboratory test results, the proposed model agreed well with the measured results. This proves the accuracy and reliability of the concrete constitutive model for simulating the time-dependent strength and stiffness of stabilized soil. It can be concluded that the role of the concrete constitutive model is to provide a framework for predicting how the mechanical properties of the stabilized soil change over time. Utilizing this model enables engineers to understand and predict how the strength and stiffness of the stabilized soil evolve over time, which is crucial for designing and evaluating the performance of engineering structures constructed on such soil in both the short term and the long term.

8. Declarations

8.1. Author Contributions

8.2. Data Availability Statement

The data presented in this study are available on request from the corresponding author.

8.3. Funding

8.4. Acknowledgements

8.5. Conflicts of Interest

The authors declare no conflict of interest.

9. References

[1] Saleh, S., Mohd Yunus, N. Z., Ahmad, K., & Mat Said, K. N. (2021). Numerical simulation with hardening soil model parameters of marine clay obtained from conventional tests. SN Applied Sciences, 3(2), 156. doi:10.1007/s42452-020-04115-w.

[2] Sabetamal, H., Sheng, D., Carter, J. (2021). Advanced Soil Constitutive Models and Their Applications to Offshore Geotechnical Problems. Challenges and Innovations in Geomechanics, IACMAG 2021, Lecture Notes in Civil Engineering, 126, Springer, Cham, Switzerland. doi:10.1007/978-3-030-64518-2_116.

[3] Onyelowe, K. C., Ebid, A. M., Ramani Sujatha, E., Fazel-Mojtahedi, F., Golaghaei-Darzi, A., Kontoni, D. P. N., & Nooralddin-Othman, N. (2023). Extensive overview of soil constitutive relations and applications for geotechnical engineering problems. Heliyon, 9(3), e14465. doi:10.1016/j.heliyon.2023.e14465.

[4] Karim, M. R., & Gnanendran, C. T. (2014). Review of constitutive models for describing the time dependent behavior of soft clays. Geomechanics and Geoengineering, 9(1), 36–51. doi:10.1080/17486025.2013.804212.

[5] Karstunen, M., & Yin, Z. Y. (2010). Modelling time-dependent behavior of Murro test embankment. Geotechnique, 60(10), 735–749. doi:10.1680/geot.8.P.027.

[6] Baskari, T. L., Zakaria, Z., Sulaksana, N., & Muljana, B. (2021). Study On Rheological Constitutive Model Of Cililin Volcanic Clay, Indonesia In Relation To Long-Term Slope Stability. International Journal of GEOMATE, 21(86), 40–47. doi:10.21660/2021.86.j2269.

[7] Teshager, D. K., & Belayneh, H. L. (2022). Reviews on Finite Element Modeling Practices of Stone Columns for Soft Soil Stabilization Beneath an Embankment Dam. Studia Geotechnica et Mechanica, 44(4), 343–353. doi:10.2478/sgem-2022-0024.

[8] Sternik, K. (2017). Elasto-plastic Constitutive Model for Overconsolidated Clays. International Journal of Civil Engineering, 15(3), 431–440. doi:10.1007/s40999-017-0193-8.

[9] Mohammed, A. S., & Vipulanandan, C. (2014). Compressive and Tensile Behavior of Polymer Treated Sulfate Contaminated CL Soil. Geotechnical and Geological Engineering, 32(1), 71–83. doi:10.1007/s10706-013-9692-9.

[10] Ikeagwuani, C. C., & Nwonu, D. C. (2019). Emerging trends in expansive soil stabilisation: A review. Journal of Rock Mechanics and Geotechnical Engineering, 11(2), 423–440. doi:10.1016/j.jrmge.2018.08.013.

[11] Jiang, Y., Han, J., & Zheng, G. (2013). Numerical analysis of consolidation of soft soils fully-penetrated by deep-mixed columns. KSCE Journal of Civil Engineering, 17(1), 96–105. doi:10.1007/s12205-013-1641-x.

[12] Tsige, D., Korita, M., & Beyene, A. (2022). Deformation analysis of cement modified soft clay soil using finite element method (FEM). Heliyon, 8(6), e09613. doi:10.1016/j.heliyon.2022.e09613.

[13] Abdullah, G. M. S., & El Aal, A. A. (2021). Assessment of the reuse of Covid-19 healthy personal protective materials in enhancing geotechnical properties of Najran's soil for road construction: Numerical and experimental study. Journal of Cleaner Production, 320, 128772 . doi:10.1016/j.jclepro.2021.128772.

[14] Jassim, N. W., Hassan, H. A., Mohammed, H. A., & Fattah, M. Y. (2022). Utilization of waste marble powder as sustainable stabilization materials for subgrade layer. Results in Engineering, 14, 100436. doi:10.1016/j.rineng.2022.100436.

[15] Negesa, A. B., Gebretsadik, H. M., & Miju, R. B. (2023). Deformation Response of Sensitive Clay Reinforced with Recycled High-Density Polyethylene Plastic Polymer Chips: Experimental and Numerical Analysis, 1-19. doi:10.2139/ssrn.4340001.

[16] Adithan, K., Neethi Chandra, A., Reddy, T. L. G., Vaishnao Vignesh, G., Sharma, A., & Ramkrishnan, R. (2021). Numerical Analysis of Soil Reinforcement using Geocell infilled with Quarry Dust Powder. Journal of Physics: Conference Series, 2070(1), 012189. doi:10.1088/1742-6596/2070/1/012189.

[17] Robin, V., Cuisinier, O., Masrouri, F., & Javadi, A. A. (2014). Chemo-mechanical modelling of lime treated soils. Applied Clay Science, 95, 211–219. doi:10.1016/j.clay.2014.04.015.

[18] Nguyen, L., Fatahi, B., & Khabbaz, H. (2016). Predicting the Behavior of Fibre Reinforced Cement Treated Clay. Procedia Engineering, 143, 153–160. doi:10.1016/j.proeng.2016.06.020.

[19] Abdullah, G. M. S. (2019). 3D finite element modeling to predict the foamed sulfur asphalt marl soil mixes rutting behavior. Ain Shams Engineering Journal, 10(4), 661–668. doi:10.1016/j.asej.2019.03.005.

[20] Li, X. (2014). Shrinkage cracking of soils and cementitiously-stabilized soils: Mechanisms and modeling. Ph.D. Thesis, Washington State University, Washington, United States.

[21] Mahvash-mohammadi, S. (2017). The Utilization of Fly Ash for Ground Improvement. Ph.D. Thesis, University of West London, London, United Kingdom.

[22] Shaalan, H. H., Azit, R., & Mohamad Ismail, M. A. (2018). Numerical Analysis of TBM Tunnel Lining Behavior using Shotcrete Constitutive Model. Civil Engineering Journal, 4(5), 1046. doi:10.28991/cej-0309155.

[23] Schütz, R., Potts, D. M., & Zdravkovic, L. (2011). Advanced constitutive modelling of shotcrete: Model formulation and calibration. Computers and Geotechnics, 38(6), 834–845. doi:10.1016/j.compgeo.2011.05.006.

[24] Paternesi, A., Schweiger, H. F., Ruggeri, P., Fruzzetti, V. M. E., & Scarpelli, G. (2017). Comparisons of Eurocodes design approaches for numerical analysis of shallow tunnels. Tunnelling and Underground Space Technology, 62, 115–125. doi:10.1016/j.tust.2016.12.003.

[25] Waichita, S., Jongpradist, P., & Schweiger, H. F. (2020). Numerical and experimental investigation of failure of a DCM-wall considering softening behavior. Computers and Geotechnics, 119, 103380. doi:10.1016/j.compgeo.2019.103380.

[26] Ong, Q.J. & Tan, S.A. (2019). Collapse of an excavation utilizing cement-treated soil columns and lessons learnt. 16th Asian Regional Conference on Soil Mechanics and Geotechnical Engineering (16th ARC), Taipei, Taiwan.

[27] Hung, H.M., Cheang, W., Long, P.D., Tuan, N.A. (2020). Simulation of Cement-Treated Soils Considering Softening Behavior. Geotechnics for Sustainable Infrastructure Development, Lecture Notes in Civil Engineering, 62, Springer, Singapore. doi:10.1007/978-981-15-2184-3_134.

[28] Maatkamp, T. W. P. (2016). The capabilities of the Plaxis Shotcrete material model for designing laterally loaded reinforced concrete structures in the subsurface. Master Thesis, Delft University of Technology, Delft, Netherlands.

[29] Çelik, S., Majedi, P., & Akbulut, S. (2019). Granular Soil Improvement by Using Polyester Grouts. Iranian Journal of Science and Technology - Transactions of Civil Engineering, 43(3), 599–606. doi:10.1007/s40996-018-0203-3.

[30] Zheng, X., & Wu, J. (2021). Early Strength Development of Soft Clay Stabilized by One-Part Ground Granulated Blast Furnace Slag and Fly Ash-Based Geopolymer. Frontiers in Materials, 8. doi:10.3389/fmats.2021.616430.

[31] Ratchakrom, C. (2019). The effect of bottom ash and kaolin on the strength of poor subbase. International Journal of GEOMATE, 16(57), 76–81. doi:10.21660/2019.57.4665.

[32] Yang, Y., Ruan, S., Wu, S., Chu, J., Unluer, C., Liu, H., & Cheng, L. (2021). Biocarbonation of reactive magnesia for soil improvement. Acta Geotechnica, 16(4), 1113–1125. doi:10.1007/s11440-020-01093-6.

[33] Soltani, A., Tarighat, A., & Varmazyari, M. (2018). Calcined Marl and Condensed Silica Fume as Partial Replacement for Ordinary Portland Cement. International Journal of Civil Engineering, 16(11), 1549–1559. doi:10.1007/s40999-018-0289-9.

[34] Ezreig, A. M. A., Ismail, M. A. M., & Ehwailat, K. I. A. (2022). A state of review: challenges and techniques of laterite soil stabilisation using chemical, economical, and eco-friendly materials. Innovative Infrastructure Solutions, 7(3), 229. doi:10.1007/s41062-022-00821-z.

[35] Gorde, P., Bendale, D., Sawkar, N., Dhonddev, S., Kanade, S., & Bhoye, D. (2024). Review on Fibres Used in Bituminous Pavement and Their Behaviors. EasyChair Preprint 11740, Manchester, United Kingdom.

[36] Fawaz, A., Alhakim, G., & Jaber, L. (2024). The stabilisation of clayey soil by using sawdust and sawdust ash. Environmental Technology, 1–11. doi:10.1080/09593330.2024.2304674.

[37] Atiqah Abdul Azam, F., Bt Che Omar, R., Bte Roslan, R., Baharudin, I. N. Z., & Muchlas, N. H. M. (2024). Enhancing the soil stability using biological and plastic waste materials integrated sustainable technique. Alexandria Engineering Journal, 91, 321–333. doi:10.1016/j.aej.2024.02.016.

[38] Mahmood, A. A., Hussain, M. K., & Ali Mohamad, S. N. (2020). Use of palm oil fuel ash (POFA)-stabilized Sarawak peat composite for road subbase. Materials Today: Proceedings, 20, 505–511. doi:10.1016/j.matpr.2019.09.178.

[39] Abdeldjouad, L., Asadi, A., Nahazanan, H., Huat, B. B. K., Dheyab, W., & Elkhebu, A. G. (2019). Effect of Clay Content on Soil Stabilization with Alkaline Activation. International Journal of Geosynthetics and Ground Engineering, 5(1), 4. doi:10.1007/s40891-019-0157-y.

[40] Sukmak, P., Sukmak, G., Horpibulsuk, S., Setkit, M., Kassawat, S., & Arulrajah, A. (2019). Palm oil fuel ash-soft soil geopolymer for subgrade applications: strength and microstructural evaluation. Road Materials and Pavement Design, 20(1), 110–131. doi:10.1080/14680629.2017.1375967.

[41] Ezreig, A. M. A., Mohamad Ismail, M. A., & Azarroug Ehwailat, K. I. (2023). Geotechnical performance of tropical laterite soil using palm oil fuel ash and activator magnesium oxide stabilizer. Physics and Chemistry of the Earth, Parts A/B/C, 129, 103293. doi:10.1016/j.pce.2022.103293.

[42] ISO 17892-4:2016. (2016). Standards Publication Geotechnical Investigation and Testing—Laboratory Testing of Soil Part 4: Determination of Particle Size. International Organization for Standardization (ISO), Geneva, Switzerland.

[43] Bozkurt, S., Abed, A., & Karstunen, M. (2023). Finite element analysis for a deep excavation in soft clay supported by lime-cement columns. Computers and Geotechnics, 162, 105687. doi:10.1016/j.compgeo.2023.105687.

[44] Fattah, M. Y., Ismael, R. H., & Aswad, M. F. (2021). Dispersion characteristics of MgO-treated dispersive clay. Arabian Journal of Geosciences, 14(7), 605. doi:10.1007/s12517-021-06957-z.

[45] Saadeldin, R., & Siddiqua, S. (2013). Geotechnical characterization of a clay-cement mix. Bulletin of Engineering Geology and the Environment, 72(3–4), 601–608. doi:10.1007/s10064-013-0531-2.

[46] Mohammed Al-Bared, M. A., & Marto, A. (2017). A review on the geotechnical and engineering characteristics of marine clay and the modern methods of improvements. Malaysian Journal of Fundamental and Applied Sciences, 13(4), 825–831. doi:10.11113/mjfas.v13n4.921.

[47] Khasib, I. A., Daud, N. N. N., & Nasir, N. A. M. (2021). Strength development and microstructural behavior of soils stabilized with palm oil fuel ash (POFA)-based geopolymer. Applied Sciences, 11(8), 3572. doi:10.3390/app11083572.

[48] Zhou, Y., Wang, Y., Yu, K., Feng, S., Zhang, H., & Zhao, J. (2023). Synergistic flame retardancy of piperazine pyrophosphate/magnesium hydroxide/fly ash cenospheres-doped rigid polyurethane foams. Construction and Building Materials, 408, 133670. doi:10.1016/j.conbuildmat.2023.133670.

[49] ASTM D2166/D2166M-16. (2013). Standard Test Method for Unconfined Compressive Strength of Cohesive Soil. ASTM International, Pennsylvania, United States. doi:10.1520/D2166_D2166M-16.

[50] Jiang, N., Wang, C., Wang, Z., Li, B., & Liu, Y. A. (2021). Strength characteristics and microstructure of cement stabilized soft soil admixed with silica fume. Materials, 14(8), 1929. doi:10.3390/ma14081929.

[51] Haeri, S. M., & Valishzadeh, A. (2021). Evaluation of Using Different Nanomaterials to Stabilize the Collapsible Loessial Soil. International Journal of Civil Engineering, 19(5), 583–594. doi:10.1007/s40999-020-00583-8.

[52] Saadat, M., & Bayat, M. (2022). Prediction of the unconfined compressive strength of stabilized soil by Adaptive Neuro Fuzzy Inference System (ANFIS) and Non-Linear Regression (NLR). Geomechanics and Geoengineering, 17(1), 80–91. doi:10.1080/17486025.2019.1699668.

[53] Wang, Y., Zhao, Y., Han, Y., & Zhou, M. (2022). The effect of circulating fluidised bed bottom ash content on the mechanical properties and drying shrinkage of cement-stabilized soil. Materials, 15(1), 14. doi:10.3390/ma15010014.

[54] Bayat, M., Asgari, M. R., & Mousivand, M. (2013). Effects of cement and lime treatment on geotechnical properties of a low plasticity clay. International Conference on Civil Engineering Architecture & Urban Sustainable Development, 27-28 November, Tabriz, Iran.

[55] Elmannaey, A. S., Fouad, H. E. E., & Youssef, Y. G. (2021). Improvement of swelling chlorite soil using sodium silicate alkali activator. Ain Shams Engineering Journal, 12(2), 1535–1544. doi:10.1016/j.asej.2020.10.019.

[56] Kim, A. R., Chang, I., Cho, G. C., & Shim, S. H. (2018). Strength and Dynamic Properties of Cement-Mixed Korean Marine Clays. KSCE Journal of Civil Engineering, 22(4), 1150–1161. doi:10.1007/s12205-017-1686-3.

[57] Gudissa Lemu, D., & Verma, R. K. (2018). Compacted Behavior of Cement Stabilized Lateritic Soil And Its Economic Benefit Over Selective Borrow Material In Road Construction: A Case Study In Wolayita Sodo. World Journal of Engineering Research and Technology WJERT, 4(2), 1-34.

[58] Saing, Z., Samang, L., Harianto, T., & Patanduk, J. (2017). Mechanical characteristic of ferro laterite soil with cement stabilization as a subgrade material. International Journal of Civil Engineering and Technology, 8(3), 609–616.

[59] Yusuf, H., Pallu, M. H., Samang, L., & Tjaronge, M. W. (2012). Characteristical analysis of unconfined compressive strength and CBR laboratory on dredging sediment stabilized with Portland cement. International Journal of Civil & Environmental Engineering, 12(04), 25-31.

[60] Pongsivasathit, S., Horpibulsuk, S., & Piyaphipat, S. (2019). Assessment of mechanical properties of cement stabilized soils. In Case Studies in Construction Materials, 11, e00301. doi:10.1016/j.cscm.2019.e00301.

[61] Wahab, N. A., Roshan, M. J., Rashid, A. S. A., Hezmi, M. A., Jusoh, S. N., Norsyahariati, N. D. N., & Tamassoki, S. (2021). Strength and durability of cement-treated lateritic soil. Sustainability, 13(11), 6430. doi:10.3390/su13116430.

[62] Eyo, E. U. (2020). Performance of expansive soils stabilized by cementitious binders and inclusion of a nanotechnology-based additive Ph.D. Thesis, Coventry University, Coventry, United Kingdom.

[63] Yong, L. L., Perera, S. V. A. D. N. J., Syamsir, A., Emmanuel, E., Paul, S. C., & Anggraini, V. (2019). Stabilization of a residual soil using calcium and magnesium hydroxide nanoparticles: A quick precipitation method. Applied Sciences, 9(20), 4325. doi:10.3390/app9204325.

[64] Al-Duais, I. N., Ahmad, S., Al-Osta, M. M., Maslehuddin, M., Saleh, T. A., & Al-Dulaijan, S. U. (2023). Optimization of alkali-activated binders using natural minerals and industrial waste materials as precursor materials. Journal of Building Engineering, 69, 106230. doi:10.1016/j.jobe.2023.106230.

[65] PLAXIS (2018). Plaxis Connect Edition V22.02 PLAXIS 2D-Reference Manual. 2D Geotechnical Engineering Software, Bentley Systems, Pennsylvania, United States.

[66] PLAXIS (2022). Plaxis Material Models Connect Edition V22.01. Bentley Systems, Pennsylvania, United States.

[67] Yu, Y., Damians, I. P., & Bathurst, R. J. (2015). Influence of choice of FLAC and PLAXIS interface models on reinforced soil–structure interactions. Computers and Geotechnics, 65, 164-174. doi:10.1016/j.compgeo.2014.12.009.

[68] Yapage, N. N. S., & Liyanapathirana, D. S. (2019). A review of constitutive models for cement-treated clay. International Journal of Geotechnical Engineering, 13(6), 525–537. doi:10.1080/19386362.2017.1370878.

[69] Vinoth, M., Prasad, P. S., & Guru Vittal, U. K. (2019). Performance analysis of PLAXIS models of stone columns in soft marine clay. Geotechnics for Transportation Infrastructure: Recent Developments, Upcoming Technologies and New Concepts, Volume 2, 557-569. doi:10.1007/978-981-13-6713-7_44.

[70] Yaro, N. S. A., Bin Napiah, M., Sutanto, M. H., Usman, A., & Saeed, S. M. (2021). Performance evaluation of waste palm oil fiber reinforced stone matrix asphalt mixtures using traditional and sequential mixing processes. Case Studies in Construction Materials, 15, e00783. doi:10.1016/j.cscm.2021.e00783.

[71] Jafer, H., Atherton, W., Sadique, M., Ruddock, F., & Loffill, E. (2018). Stabilisation of soft soil using binary blending of high calcium fly ash and palm oil fuel ash. Applied Clay Science, 152, 323-332. doi:10.1016/j.clay.2017.11.030.

[72] Ghiasi, V., & Eskandari, S. (2023). Comparing a single pile's axial bearing capacity using numerical modeling and analytical techniques. Results in Engineering, 17, 100893. doi:10.1016/j.rineng.2023.100893.

[73] Tang, Q., Shi, P., Zhang, Y., Liu, W., & Chen, L. (2019). Strength and Deformation Properties of Fiber and Cement Reinforced Heavy Metal-Contaminated Synthetic Soils. Advances in Materials Science and Engineering, 2019, 1–9. doi:10.1155/2019/5746315.

[74] Ho, T. O., Chen, W. B., Yin, J. H., Wu, P. C., & Tsang, D. C. W. (2021). Stress-Strain behavior of Cement-Stabilized Hong Kong marine deposits. Construction and Building Materials, 274, 122103. doi:10.1016/j.conbuildmat.2020.122103.

[75] Wang, Z., Zhang, W., Jiang, P., & Li, C. (2022). The Elastic Modulus and Damage Stress–Strain Model of Polypropylene Fiber and Nano Clay Modified Lime Treated Soil under Axial Load. Polymers, 14(13), 2606. doi:10.3390/polym14132606.

[76] Miturski, M., Głuchowski, A., & Sas, W. (2021). Influence of dispersed reinforcement on mechanical properties of stabilized soil. Materials, 14(20), 5982. doi:10.3390/ma14205982.

[77] Jeremiah, J. J., Abbey, S. J., Booth, C. A., & Kashyap, A. (2021). Geopolymers as Alternative Sustainable Binders for Stabilisation of Clays—A Review. Geotechnics, 1(2), 439–459. doi:10.3390/geotechnics1020021.

[78] Mahvash-Mohammadi, S. (2017) The utilization of fly ash for ground improvement: a sustainable construction of embankment. Ph.D. Thesis, University of West London, London, United Kingdom.

[79] Shaalan, H., Mohamad Ismail, M. A., & Azit, R. (2018). Application of shotcrete constitutive model to the time dependent behavior of TBM tunnel lining. International Journal of Engineering & Technology, 7(3), 1826. doi:10.14419/ijet.v7i3.11293.

[80] Shaalan, H., Ismail, M. A. M., & Azit, R. (2016). Time-dependency behavior of steel fiber reinforced shotcrete lining under rock overstressing using shotcrete model. Electronic Journal of Geotechnical Engineering, 21(26), 10365–10378.